

# Prediction of high $zT$ in thermoelectric silicon nanowires with axial germanium heterostructures

M. SHELLEY and A. A. MOSTOFI<sup>(a)</sup>

*The Thomas Young Centre for Theory and Simulation of Materials, Imperial College London, London SW7 2AZ, UK*

PACS 73.63.Nm – Quantum wires

PACS 72.20.Pa – Thermoelectric and thermomagnetic effects

PACS 63.22.Gh – Nanotubes and nanowires

**Abstract** – We calculate the thermoelectric figure of merit,  $zT = S^2GT/(\kappa_l + \kappa_e)$ , for  $p$ -type Si nanowires with axial Ge heterostructures using a combination of first-principles density-functional theory, interatomic potentials, and Landauer-Buttiker transport theory. We consider nanowires with up to 8400 atoms and twelve Ge axial heterostructures along their length. We find that introducing heterostructures always reduces  $S^2G$ , and that our calculated increases in  $zT$  are predominantly driven by associated decreases in  $\kappa_l$ . Of the systems considered,  $\{111\}$  nanowires with a regular distribution of Ge heterostructures have the highest figure-of-merit:  $zT = 3$ , an order of magnitude larger than the equivalent pristine nanowire. Even in the presence of realistic structural disorder, in the form of small variations in length of the heterostructures,  $zT$  remains several times larger than that of the pristine case, suggesting that axial heterostructuring is a promising route to high- $zT$  thermoelectric nanowires.

In recent years, silicon nanowires (SiNWs) have been proposed for use as chemical sensors [1], photovoltaics [2] and thermoelectrics [3,4]. Hicks and Dresselhaus [5] first identified that NWs could be used to improve the thermoelectric figure of merit,  $zT$ , over bulk and two-dimensional superlattice (2DSL) values. While the dramatic increases that were predicted have not been yet realised, much progress has been made: Refs. [3,4] report  $zT \sim 1$  for SiNWs, a 100-fold increase over the value for bulk Si.

The measure of the performance of a thermoelectric material is given by its figure of merit  $zT = S^2GT/(\kappa_l + \kappa_e)$ , where  $S$ ,  $G$  and  $T$  are the Seebeck co-efficient, electronic conductance and average temperature of the two contacts, respectively, and  $\kappa_l$  and  $\kappa_e$  are the lattice and electronic contributions to the thermal conductance, respectively.  $zT$  may, therefore, be increased by designing materials that have either higher thermoelectric power factor  $S^2G$ , or lower thermal conductivity. The relatively high  $zT$  seen in recent experiments on SiNWs has been attributed to both of these effects: an increase in  $S$  resulting from enhanced phonon drag [4], and a decrease in  $\kappa_l$  resulting from surface scattering of phonons [3,6].

By analogy with 2DSLs, which show a reduction in  $\kappa_l$  compared to its value both in the bulk and in the alloy limit [7], superlatticed NWs have been proposed as a possible route toward high  $zT$  thermoelectrics [8], through both enhancement of the power factor  $S^2G$  and reduction of  $\kappa_l$ , as compared to pristine NWs. Experimental evidence for Si-SiGe

<sup>(a)</sup>Email: a.mostofi@imperial.ac.uk

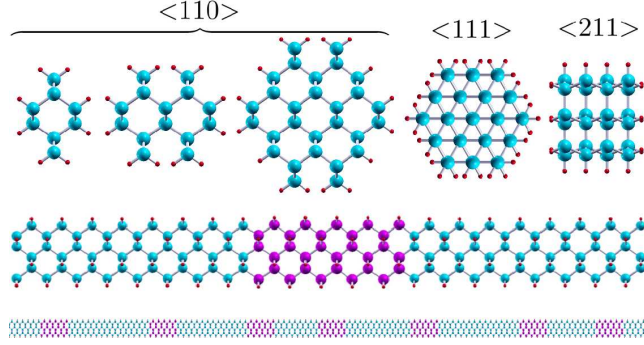


Fig. 1: Top: Cross-sections of SiNWs. Labels indicate the crystal direction of the longitudinal ( $z$ ) axis (pointing into the page). Diameters (left-to-right): 0.78 nm, 1.02 nm, 1.44 nm, 1.14 nm and 1.06 nm. Middle: A single Ge heterostructure in a SiNW (Ge and Si atoms in magenta and blue, respectively). Bottom: A multiple heterostructure nanowire (MHNW) with an arbitrary distribution of Ge heterostructures.

NWs [9] supports the idea that superlattice results in a reduction in  $\kappa_L$ , although direct experimental evidence for increased  $S^2G$  is still missing.

In this Letter, we use a combination of first-principles density-functional theory simulations and calculations with interatomic potentials in order to compute  $zT$  for axially heterostructured Si-Ge NWs within the coherent transport regime using the Landauer-Buttiker approach [10,11]. More specifically, we calculate  $zT$  at 300 K for thin ( $< 2$  nm diameter),  $p$ -type  $\langle 110 \rangle$ ,  $\langle 111 \rangle$  and  $\langle 211 \rangle$  H-passivated SiNWs (Fig. 1, top) containing: (a) single axial Ge heterostructures with lengths ranging from 0.4 nm to 4.3 nm (Fig. 1, middle); (b) multiple Ge heterostructures of uniform length, distributed along the length of the NW either randomly, periodically, or as a Fibonacci chain (Fig. 1, bottom); and (c) multiple Ge heterostructures whose lengths approximately follow a Gaussian distribution.

Our calculations demonstrate that: (i) the introduction of a single Ge heterostructure in a SiNW can lead to a 3.5-fold increase in  $zT$  as compared to the equivalent pristine SiNW; (ii) this can be further enhanced to a 7.4-fold increase by introducing multiple Ge heterostructures and by controlling their spatial distribution along the length of the SiNW; (iii) this observed enhancement in  $zT$  is almost entirely due to a reduction in thermal conductivity rather than an increase in the power factor  $S^2G$  – indeed, we find that introducing Ge heterostructures in an SiNW always results in a decrease in  $S^2G$ ; and (iv) introducing further disorder, in the form of a variability in the length of the Ge heterostructures within a SiNW, results in a decrease in  $zT$  as compared to the case in which the heterostructures are all identical, highlighting the importance of precise atomic-scale control that may be required in order to fabricate high- $zT$  NWs.

Our method (described in detail elsewhere [12]), in which accurate yet compact model Hamiltonians of large-scale systems are constructed from first-principles calculations, enables us to study transport through meso-scale systems with modest computational cost: our largest simulations consist of a conductor region of length 116 nm (8432 atoms) coupled to semi-infinite leads. Our procedure is largely automated, which has made it possible to perform high-throughput calculations and undertake a comprehensive study of a large structural parameter space. With little modification, our general approach may be easily used to calculate transport properties in other quasi one-dimensional systems.

We note that analogous approaches have been used recently for calculating electronic and/or thermal transport in large-scale 1D systems, e.g., in SiNWs [13,14] and carbon nanotubes [15–17].

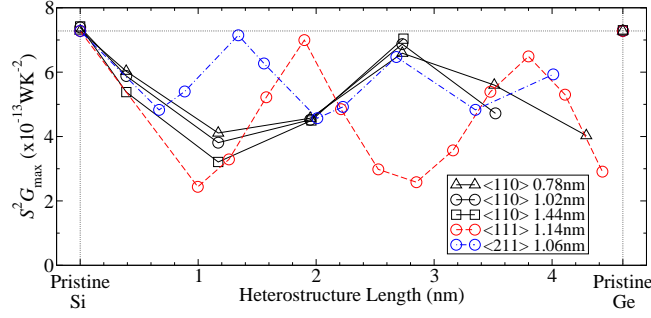


Fig. 2: Maximum thermoelectric power factor  $S^2 G_{\max}$  at 300 K for single Ge heterostructures in  $\langle 110 \rangle$  (black solid lines),  $\langle 111 \rangle$  (red dashed lines) and  $\langle 211 \rangle$  (blue dot-dashed lines) SiNWs. Three diameters 0.78 nm (triangles), 1.02 nm (circles) and 1.44 nm (squares) are shown for the  $\langle 110 \rangle$  direction. Pristine SiNWs are shown plotted as zero heterostructure length and pristine Ge NWs values are shown on the right.

**Electronic transport properties.** – Starting from a plane-wave density-functional theory (PW-DFT) calculation<sup>1</sup>, a unitary transformation is applied to the extended ground state eigenfunctions in order to obtain maximally-localized Wannier functions (MLWFs) [20] and, hence, the Hamiltonian matrix in the basis of MLWFs. Due to the localized nature of MLWFs in real-space, the Hamiltonian matrix can be spatially partitioned and used in so-called “lead-conductor-lead” Landauer-Buttiker [10, 11] transport calculations, using standard Green function techniques [12, 21–24]. In our case, the semi-infinite “leads” are pristine (H-passivated) SiNWs and the central “conductor” region comprises of SiNW with some axial distribution of Ge heterostructures. An example of such a system exhibiting a single Ge heterostructure is shown in Fig. 1 (middle panel). Although we begin with PW-DFT calculations with periodic boundary conditions, we determine electronic transport properties under open boundary conditions. Once the electronic density of states of the conductor and the transmission function  $\mathcal{T}(\epsilon)$  are calculated, one can write [25, 26]  $G = e^2 L_0(\mu)$ ,  $S = L_1(\mu)/eTL_0(\mu)$  and  $\kappa_e = \frac{1}{T} \{L_2(\mu) - [L_1(\mu)]^2/L_0(\mu)\}$ , where

$$L_m(\mu) = \frac{2}{h} \int_{-\infty}^{\infty} \mathcal{T}(\epsilon) (\epsilon - \mu)^m \left( \frac{-\partial f(\epsilon, \mu)}{\partial \epsilon} \right) d\epsilon, \quad (1)$$

and  $f(\epsilon, \mu) = 1/\{\exp[(\epsilon - \mu)/k_B T] + 1\}$  is the Fermi-Dirac function at chemical potential  $\mu$ . In this Letter, we focus on hole transport, so that we can associate  $\mu$  with a carrier concentration that is driven by  $p$ -doping<sup>2</sup>.

As full DFT structural relaxation of our large heterostructured NWs would have been computationally intractable, the atomic configurations used for the electronic calculations were built by piecing together unit cells of pristine Si and Ge NWs whose equilibrium lattice parameters<sup>3</sup> were calculated separately with DFT. For the smallest NWs considered, the results obtained from our approach had only small quantitative and no qualitative difference as compared to those from the equivalent fully relaxed structure [19].

Fig. 2 shows the maximum<sup>4</sup> thermoelectric power factor  $S^2 G_{\max}$  for a range of Ge

<sup>1</sup>We use the Quantum-Espresso package [18], the local-density approximation for exchange and correlation, norm-conserving pseudopotentials, a 400 eV energy cut-off for the PW basis set, and  $\Gamma$ -point sampling of the Brillouin zone.

<sup>2</sup>This doping is ‘artificial’ in the sense that we do not directly include dopant atoms in our calculation.

<sup>3</sup>These were 3.775 Å (3.910 Å), 9.224 Å (9.497 Å), and 6.470 Å (6.692 Å), for our largest diameter Si (Ge) NWs in the  $\langle 110 \rangle$ ,  $\langle 111 \rangle$  and  $\langle 211 \rangle$  growth directions, respectively.

<sup>4</sup>As can be seen from Eq. (1), the electronic transport coefficients are functions of chemical potential  $\mu$ . Throughout this work,  $S^2 G_{\max}$  and  $zT_{\max}$  are defined to be the maximum values of the power factor and the figure of merit, respectively, as a function of  $\mu$ . The maximal power factors shown in Fig. 2 are obtained, in all cases, for values of  $\mu$  within 30 meV of the Si valence band edge.

heterostructure lengths in  $\langle 110 \rangle$  (black solid lines),  $\bar{1}11$  (red dashed line) and  $\langle 211 \rangle$  (blue dot-dashed line) SiNWs. We note first that in no case does the introduction of an axial heterostructure result in an increase of  $S^2G_{\max}$ , the value of which is, at best, approximately the same as that of a pristine SiNW. The similarity of the results between pristine SiNWs and GeNWs is also interesting to note. Since all the NWs investigated only have a single channel that is available for conduction at the top of the valence manifold, we confirm that the most important factor for  $S^2G_{\max}$  in quasi-one-dimensional systems is the number of conducting channels at this edge [27].

The oscillations in Fig. 2 can be explained by a model in which the heterostructure is considered as a 1D quantum potential well of width  $L$ , corresponding to the length of the heterostructure, and depth  $V_0$ , corresponding to the band offset between Si and Ge. The reflection amplitude of a wave incident on such a well vanishes when the well-known Fabry-Perot resonance condition is satisfied,  $qL = n\pi$ , where  $q$  is the wavevector inside the well and  $n$  is an integer. For holes entering the heterostructure, this condition gives  $E_n(L) = -\frac{\hbar^2}{2m^*} \frac{n^2}{L^2} + V_0$ , where  $m^*$  is the effective mass of holes and  $E_n(L)$  are energies at which resonances occur in the transmission. For the  $\bar{1}11$  NWs, which show the strongest oscillations in  $S^2G_{\max}$ , plotting the resonance energies against  $1/L^2$  produces an excellent linear fit (not shown), with correlation coefficient  $r^2 = 0.998$ , giving  $m^* = 0.28 m_e$  and  $V_0 = 0.32$  eV. Models such as this may be a useful additional tool for the optimization of heterostructure lengths in thermoelectric devices [28].

**Phononic transport properties.** — We determine the lattice thermal conductance  $\kappa_l$  in an analogous way to the electronic conductance, by segmenting the system into a lead-conductor-lead geometry. Instead of finding the Green function of a Schrödinger-type eigenvalue problem, we determine the Green function that solves the eigenvalue problem relating nuclear displacements  $u$  to the dynamical matrix  $K$  and phonon frequency  $\omega$ :  $Ku = \omega^2 u$ . Applying the thermal equivalent of the Caroli formula [21, 29], we obtain the phonon transmission function,  $\mathcal{T}(\omega)$ , in the limit of non-interacting phonons and coherent phonon transport. One can then write [30]

$$\kappa_l = \frac{\hbar^2}{2\pi k_B T^2} \int_0^\infty \mathcal{T}(\omega) \omega^2 \frac{e^{\hbar\omega/k_B T}}{(e^{\hbar\omega/k_B T} - 1)^2} d\omega. \quad (2)$$

Determination of the dynamical matrix using first-principles methods is computationally intractable for the large NW supercells with heterostructures that are considered here. To structurally relax the NWs and obtain their dynamical matrices, therefore, we use Tersoff potentials [31], which have been shown to give accurate values for lattice thermal conductivities for thin pristine SiNWs, as compared to DFT calculations [32]. It is worth noting that the approach outlined above neglects Umklapp scattering, which would further decrease  $\kappa_l$  at the temperature with which we are concerned (300 K).

Results for  $\kappa_l$  are shown in Fig. 3 (top panel) for the same single Ge heterostructure SiNWs discussed earlier. We find that, by introducing a single Ge heterostructure, the lattice thermal conductivity can be reduced by a factor of five for the  $\bar{1}11$  growth direction, as compared to the corresponding pristine SiNW, giving a value of  $0.1 \text{ nWK}^{-1}$ . Reductions in the  $\langle 110 \rangle$  and  $\langle 211 \rangle$  direction are also significant (approximately a factor of four). We tentatively suggest that the longer unit cell in the  $\bar{1}11$  direction may account for the greater reduction seen in that growth direction. It may also be seen that, in the  $\langle 110 \rangle$  direction,  $\kappa_l$  increases with diameter as more phonon modes become available. We also observe this trend in larger diameter pristine SiNWs in the  $\bar{1}11$  and  $\langle 211 \rangle$  directions (results not shown).

**$zT$  for SiNWs with a single Ge heterostructure.** — Fig. 3 (bottom panel) combines our results for electronic and phononic transport coefficients for the single Ge heterostructure systems discussed above and shows our calculated values of  $zT_{\max}$  as a function of heterostructure length. It can be seen that heterostructured SiNWs in the  $\bar{1}11$  direction

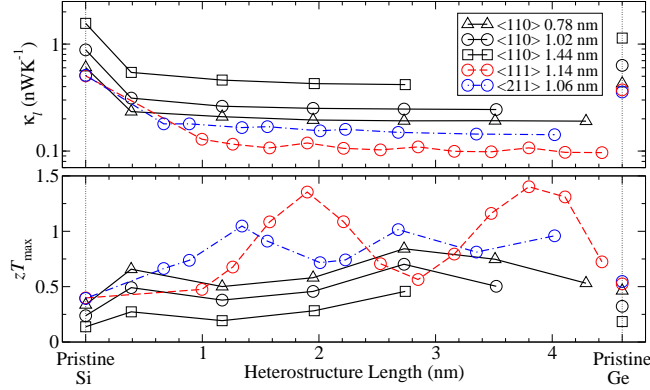


Fig. 3: Dependence of  $\kappa_l$  (top panel) and  $zT_{\max}$  (bottom panel) at 300 K as a function of Ge heterostructure length for  $\langle 110 \rangle$ ,  $\langle 111 \rangle$  and  $\langle 211 \rangle$  SiNWs. Labelling is equivalent to Fig. 2, again plotting pristine SiNWs as zero heterostructure length and pristine Ge NWs also shown on the right.

display the greatest values of the figure of merit  $zT_{\max} \simeq 1.4$ . Such high values, however, are not found consistently across the range of heterostructures studied. Such variations may limit the values of  $zT$  observed in realistic SiNWs since experimental control over heterostructure length is, currently at least, limited to length-scales comparable to, or greater than, the differences in length that are investigated here [33]. In the  $\langle 110 \rangle$  and  $\langle 211 \rangle$  directions, we find  $zT_{\max} < 1$ , mainly due to the higher lattice thermal conductivities found in these systems. We note that, across the range of systems studied, the ratio of lattice and electronic thermal conductances,  $\kappa_l/\kappa_e$ , lies between 3 and 10, therefore,  $\kappa_l$  is the dominant contribution to the denominator of  $zT$ . This emphasizes the importance of reducing the lattice thermal conductivity for high  $zT$  NWs.

**$zT$  for SiNWs with multiple Ge heterostructures.** – Next, we consider much longer SiNWs with many Ge heterostructures along their length. Such multiple heterostructure nanowires (MHNWs) are shown schematically in Fig. 4. These systems are too large for brute-force PW-DFT calculations. Instead, we use the Hamiltonian matrices of single heterostructure calculations as “building-blocks” for constructing model Hamiltonians of much larger (up to  $\simeq 8400$  atom) MHNWs, with negligible loss of accuracy. Our approach, which relies on exploiting the nearsightedness of electronic structure that becomes manifest when Hamiltonian matrices are represented in a basis of MLWFs, is described in detail in Ref. [12].

Once the model Hamiltonian for the MHNW is constructed, the electronic transport properties under open boundary conditions are calculated in exactly the same way as described above for SiNWs with single Ge heterostructures. For the lattice thermal conductivity, an analogous “building-block” scheme is used in which the (short-ranged) dynamical matrices of the single heterostructures that comprise the MHNWs are combined to construct dynamical matrices for the MHNWs. Under the assumption that phonons remain phase coherent across the length of the MHNW, this dynamical matrix is then used to calculate the phonon transmission function  $\mathcal{T}(\omega)$  and, hence, the coherent lattice thermal conductance  $\kappa_l^{\text{coh}}$  according to Eq. (2).

It is unclear whether the phase coherence length of phonons is comparable to the lengths of the MHNW systems that we consider (up to  $\simeq 116$  nm). Therefore, we also calculate the lattice thermal conductance in an ohmic regime,  $\kappa_l^{\text{ohm}}$ , in which the total resistance of a given MHNW is the sum of the thermal resistances of each individual heterostructure that constitutes the MHNW [34]. For a NW with  $N$  heterostructures, each of which in isolation

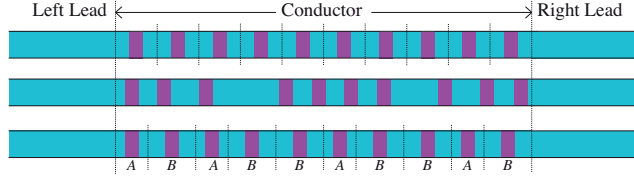


Fig. 4: Schematic illustration of MHNWs studied. Top: periodic conductor; middle: a typical random arrangement; bottom: Fibonacci chain pattern, with units  $A$  and  $B$  (see text). Si and Ge sections are in blue and magenta, respectively.

gives a transmission  $\mathcal{T}_i(E)$ , we compute the transmission function as [35]

$$\mathcal{T}^{\text{ohm}}(E) = \frac{\overline{\mathcal{T}}}{N - (1 - N)\overline{\mathcal{T}}/\mathcal{T}_0}, \quad (3)$$

where  $\overline{\mathcal{T}} = \sum_{i=1}^N \mathcal{T}_i/N$  is the average transmission of the isolated heterostructures, and  $\mathcal{T}_0$  is the transmission for the pristine NW. Having obtained  $\mathcal{T}^{\text{ohm}}(E)$ ,  $\kappa_l^{\text{ohm}}$  is calculated from Eq. (2).  $\kappa_l^{\text{coh}}$  and  $\kappa_l^{\text{ohm}}$  are used to estimate upper and lower bounds for  $zT$ .

We consider MHNWs in the  $\langle 111 \rangle$  and  $\langle 211 \rangle$  growth directions, with diameters of 1.14 nm and 1.06 nm, respectively, and Ge heterostructure lengths of 3.80 nm and 1.34 nm, respectively. For each of these two growth directions, three qualitatively distinct heterostructure distributions are considered (shown in Fig. 4): (i) random, (ii) periodic, and (iii) Fibonacci chain<sup>5</sup>, each with ten heterostructures along the length of the NW. Structural details are given in Table 1. For MHNWs with a random distribution of heterostructures,  $\mathcal{T}(\epsilon)$  and  $\mathcal{T}(\omega)$  are ensemble averaged over 250 independent configurations.

Fig. 5 (top panel) shows the thermal conductances of the MHNWs detailed in Table 1 and compares them to the pristine values. A prominent feature is the large reduction of  $\kappa_l$  due to heterostructuring, with  $\langle 111 \rangle$  MHNWs displaying smaller values than  $\langle 211 \rangle$ . Using the coherent model (red solid bars/blue bold striped bars),  $\kappa_l$  is reduced by factors of between five and eight when compared to the pristine results and reduces as the disorder is increased (periodic to Fibonacci to random patterning). The ohmic model (red shading/fine blue stripes), results in reductions of  $\kappa_l$  by factors of  $\simeq 12$  and 8.5 in  $\langle 111 \rangle$  and  $\langle 211 \rangle$  MHNWs,

<sup>5</sup>A Fibonacci chain is an example of a 1D quasicrystal [36]: it displays local translational symmetries, yet remains aperiodic *in toto*. Exceptionally low  $\kappa_l$  values have been reported experimentally for 3D quasicrystals [37], thus the introduction a Fibonacci chain distribution of heterostructures could be a systematic method to reduce  $\kappa_l$ . The Fibonacci chain MHNWs are designed such that the length ratio of structural units  $A$  and  $B$  that comprise them is as close as possible to the golden ratio  $(1 + \sqrt{5})/2$ . These structural units each contain a Ge heterostructure between lengths of SiNW and the total chain is built with three iterations ( $n = 0, 1, 2$ ) of the sequence:  $A_{n+1} = A_n B_n$ ,  $B_{n+1} = A_n$ , with  $A_0 = A$  and  $B_0 = B$ .

		$\langle 111 \rangle$	$\langle 211 \rangle$
Single heterostructure length (nm)		3.80	1.34
Periodic	Total MHNW length (nm)	93.3	50.9
	Total number of atoms	7208	3608
Random	Total MHNW length (nm)	93.3	49.6
	Total number of atoms	7208	3520
Fibonacci	Total MHNW length (nm)	93.3	49.6
	Total number of atoms	7208	3520

Table 1: Structural details of the MHNWs in the  $\langle 111 \rangle$  and  $\langle 211 \rangle$  growth directions. The different MHNWs (periodic, Fibonacci and random) are built by placing ten single heterostructures along the length of the wire.



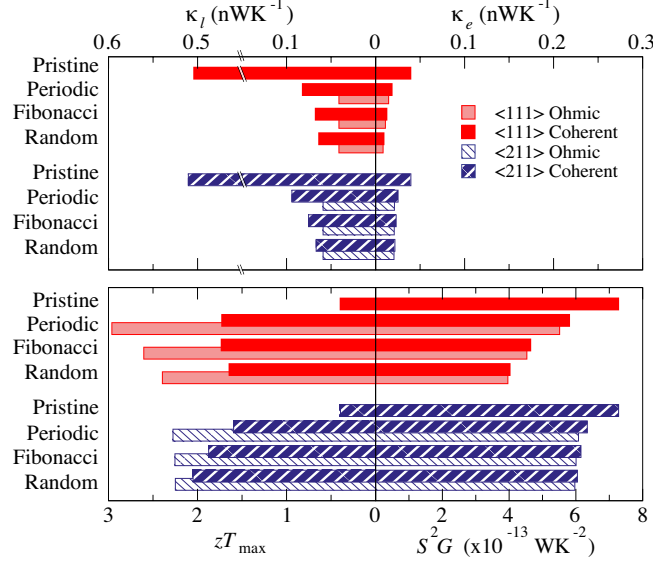


Fig. 5: Transport properties at 300 K of  $\bar{1}11$  (red, solid bars) and  $\langle 211 \rangle$  (blue, striped bars) periodic, Fibonacci and random patterned MHNWs, and comparison to the pristine cases. Results from fully coherent phononic transport  $\bar{1}11$  ( $\langle 211 \rangle$ ) calculations have solid shading (bold stripe), while results in the ohmic regime have a lighter shading (fine stripe). Top panel: the lattice (left) and electronic (right) contributions to the thermal conductance, respectively. Bottom panel:  $zT_{\max}$  (left) and  $S^2G$  (right) at the value of  $\mu$  that maximizes  $zT$  for each system.

respectively. We note that  $\kappa_l^{\text{coh}}/\kappa_e$  and  $\kappa_l^{\text{ohm}}/\kappa_e$  are found to be between 2.5 and 7 — only marginally smaller than those values we obtained for single heterostructure NWs.

$zT_{\max}$  and  $S^2G$  are shown in Fig. 5 (bottom panel).<sup>6</sup> It is striking that in no case does  $S^2G$  increase due to heterostructuring, and the  $\langle 211 \rangle$  direction performs best over the range of MHNWs considered, showing only small decreases (with respect to pristine) as the disorder increases from periodic to random. Together with the pronounced effect that increased disorder has on  $\kappa_l^{\text{coh}}$ , we see that, in the coherent regime, random patterning results in values of the figure of merit as high as  $zT = 2$ . Conversely,  $\bar{1}11$  MHNWs display significant reductions in  $S^2G$  as the disorder increases, which tend to counteract similar decreases in  $\kappa_l^{\text{coh}}$ , leaving  $zT_{\max}$  approximately constant at  $\simeq 1.7$ . In both  $\bar{1}11$  and  $\langle 211 \rangle$  MHNWs the calculated  $zT_{\max}$  increases if the thermal transport is assumed to be ohmic, since  $\kappa_l^{\text{ohm}} < \kappa_l^{\text{coh}}$ . In this regime,  $\kappa_l^{\text{ohm}}$  is invariant with respect to the distribution of heterostructures, therefore,  $zT_{\max}$  in this regime will follow the behaviour seen in  $S^2G$  with a value of  $zT = 2.3$  for the  $\langle 211 \rangle$  direction (almost independent of the distribution of heterostructures), and up to  $zT = 3$  in the  $\bar{1}11$  direction, with a periodic arrangement of heterostructures.

**The effect of variability of heterostructure length.** — The MHNWs that we have discussed thus far consist of multiple instances of identical heterostructures. Experimental synthesis techniques do not have this level of atomic precision, therefore, we have investigated the effect of introducing some variability of the lengths of the heterostructures that comprise the MHNW. In particular, we compare periodic patterned MHNWs with identical heterostructures with ‘near-periodic’ MHNWs that are comprised of heterostructures whose lengths are Gaussian distributed about a mean length that is given by the heterostructure

<sup>6</sup>The electronic properties are always calculated within a fully coherent model but, depending on whether  $\kappa_l^{\text{ohm}}$  or  $\kappa_l^{\text{coh}}$  is used, the value of  $\mu$  at which  $zT_{\max}$  occurs changes slightly and, hence, the value of  $S^2G$ , which is dependent on  $\mu$ .

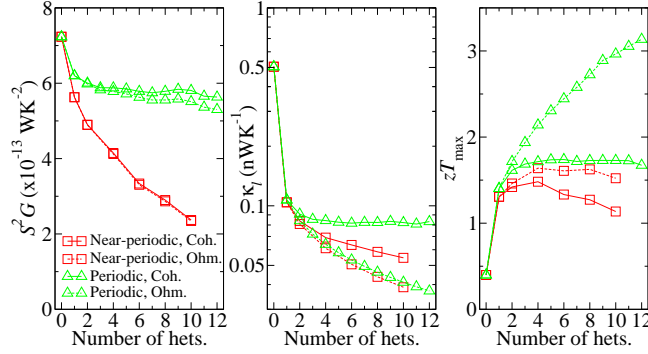


Fig. 6: Comparison of  $S^2G$  (left panel),  $\kappa_l$  (middle panel) and  $zT_{\max}$  (right panel) at 300 K in periodic (green triangles) and near-periodic (red squares)  $\bar{1}11$  MHNWs as a function of the number of Ge heterostructures (hets.). Results using the coherent (coh.) and ohmic (ohm.) phonon transport models are shown with solid and dashed lines respectively.

length used in the ‘true’ periodic case, with a standard deviation  $\sigma$  that corresponds to approximately 1/3 (1/2) a unit cell in the  $\bar{1}11$  ( $\langle 211 \rangle$ ) direction. For the near-periodic MHNWs, the transmission functions are ensemble averaged over 250 independent configurations of the disorder to model a ‘typical’ MHNW of this type.

We consider MHNWs with up to twelve heterostructures along their length. Fig. 6 shows a comparison between near-periodic (red squares) and periodic (green triangles) MHNWs in the  $\bar{1}11$  growth direction. The resulting values for  $zT_{\max}$  are shown in the right panel. In the ohmic phonon transport regime (dashed lines), the near-periodic system displays a dramatic reduction in  $zT_{\max}$  as compared to the periodic case, which arises from the sharp reduction that is found in  $S^2G$  (left panel), combined with the fact that  $\kappa_l$  does not decrease very much (middle panel). When considering the coherent regime (solid lines), the reduction in  $S^2G$  for the near-periodic MHNW is also large (left panel), as compared to the periodic MHNW, but associated decreases in  $\kappa_l$  are also observed (middle panel) so that the resultant drop in  $zT_{\max}$  (right panel), as compared to the periodic case, is much less pronounced. For the near-periodic MHNWs, both phonon transport regimes display a maximum in  $zT_{\max}$  with respect to heterostructure length after the introduction of approximately four heterostructures.

We note that the significant decreases in  $S^2G$  due to the variability in the heterostructure length is consistent with our earlier conclusion that increased disorder tends to reduce the power factor, as was seen when comparing periodic, Fibonacci and random distributions. We also note that in the ohmic phonon transport regime, there is little difference in  $\kappa_l$  between periodic and near-periodic MHNWs, which follows the earlier observation that there is almost no dependence of  $\kappa_l$  on heterostructure length in single heterostructure NWs (Fig. 3, top panel).

Finally, comparing near-periodic MHNWs in the  $\bar{1}11$  and  $\langle 211 \rangle$  growth directions, we find that  $S^2G^{(\bar{1}11)} < S^2G^{(\langle 211 \rangle)}$ , which may have been expected from the stronger dependence of  $S^2G_{\max}$  on heterostructure length in  $\bar{1}11$  SiNWs with a single heterostructure (Fig. 2). We also find that  $\kappa_l^{(\bar{1}11)} < \kappa_l^{(\langle 211 \rangle)}$ , which also could have been predicted from the trends observed for single heterostructure SiNWs (Fig. 3). However, the delicate balance between  $S^2G$  and  $\kappa_l$  make it difficult to use calculations on SiNWs with a single heterostructure to predict trends in  $zT_{\max}$  for our near-periodic MHNWs, highlighting the need for accurate first-principles approaches. Among the near-periodic MHNWs studied, the  $\bar{1}11$  direction with four heterostructures performed best, with  $zT \simeq 1.5 - 1.6$ .

In conclusion, we have performed first-principles calculations on thin,  $p$ -type  $\langle 110 \rangle$ ,  $\bar{1}11$  and  $\langle 211 \rangle$  SiNWs with Ge heterostructures. In all cases studied, a decrease of thermoelectric power factor  $S^2G$  is observed when a heterostructure is introduced, and any increase in the



figure of merit  $zT$  is due to a corresponding reduction in  $\kappa_l$ . We have built model Hamiltonians for MHNWs with over 8400 atoms while retaining first-principles accuracy. A similar method was applied to the dynamical matrices of MHNWs to obtain the thermal conductance  $\kappa_l$  for such structures. In such MHNWs we again find that  $S^2G$  is always reduced and that increases in  $zT$  are driven predominantly by significant decreases in  $\kappa_l$ . We find values as high as  $zT = 3$  in 111 MHNWs with periodic arrangements of Ge heterostructures. The intricate balance between  $S^2G$  and  $\kappa_l$ , however, makes  $zT$  strongly dependent on the details of the system at the atomic level: in structures that model the kind of disorder that may be present in realistic MHNWs, more modest values of  $zT = 1.6$  are found, which is still a factor of four greater than the pristine SiNW case. Our calculations suggest axial heterostructuring to be a promising route to high- $zT$  nanowire thermoelectrics.

\* \* \*

We are grateful to the High Performance Computing Facility at Imperial College London, and to the EPSRC and E.ON's International Research Initiative. We thank N. Poilvert, N. Marzari and Y.-S. Lee for discussions.

#### REFERENCES

- [1] CUI Y., WEI Q., PARK H. and LIEBER C. M., *Science*, **293** (2001) 1289.
- [2] GARNETT E. and YANG P., *Nano Lett.*, **10** (2010) 1082.
- [3] HOCHBAUM A. I., CHEN R., DELGADO R. D., LIANG W., GARNETT E. C., NAJARIAN M., MAJUMDAR A. and YANG P., *Nature*, **451** (2008) 163.
- [4] BOUKAI A. I., BUNIMOVICH Y., TAHIR-KHELI J., YU J.-K. GODDARD III W. A. and HEATH J. R., *Nature*, **451** (2008) 168.
- [5] HICKS L. D. and DRESSELHAUS M. S., *Phys. Rev. B*, **47** (1993) 16631.
- [6] LI D., WU Y., KIM P. SHI L., YANG P. and MAJUMDAR A., *Appl. Phys. Lett.*, **83** (2003) 2934.
- [7] BORCA-TASCIUC T. *et al.*, *Superlattices Microstruct.*, **28** (2000) 199.
- [8] LIN Y.-M. and DRESSELHAUS M. S., *Phys. Rev. B*, **68** (2003) 075304.
- [9] LI D., WU Y., FAN R., YANG P. and MAJUMDAR A., *Appl. Phys. Lett.*, **83** (2003) 3186.
- [10] LANDAUER R., *Phil. Mag.*, **21** (1970) 853.
- [11] BUTTIKER M., IMRY Y., LANDAUER R. and PINHAS S., *Phys. Rev. B*, **31** (1985) 6207.
- [12] SHELLEY M., MOSTOFI A. A., POILVERT N. and MARZARI N., <http://arxiv.org/abs/1101.3754>, (2011) .
- [13] MARKUSSEN T., RURALI R., BRANDBYGE M. and JAUHO A.-P., *Phys. Rev. B*, **74** (2006) 245313.
- [14] MARKUSSEN T., JAUHO A.-P. and BRANDBYGE M., *Phys. Rev. Lett.*, **103** (2009) 055502.
- [15] LEE Y.-S., NARDELLI M. B. and MARZARI N., *Phys. Rev. Lett.*, **95** (2005) 076804.
- [16] ROCHA A. R., ROSSI M., FAZZIO A. and DA SILVA A. J. R., *Phys. Rev. Lett.*, **100** (2008) 176803.
- [17] SAVIC I., MINGO N. and STEWART D. A., *Phys. Rev. Lett.*, **101** (2008) 165502.
- [18] GIANNOZZI P., BARONI S., BONINI N., CALANDRA M., CAR R., CAVAZZONI C., CERESOLI D., CHIAROTTI G. L., COCCIONI M., DABO I., CORSO A. D., DE GIRONCOLI S., FABRIS S., FRATESI G., GEBAUER R., GERSTMANN U., GOUGOUSSIS C., KOKALJ A., LAZZERI M., MARTIN-SAMOS L., MARZARI N., MAURI F., MAZZARELLO R., PAOLINI S., PASQUARELLO A., PAULATTO L., SBRACCIA C., SCANDOLO S., SCHLAUZERO G., SEITSONEN A. P., SMOGUNOV A., UMARI P. and WENTZCOVITCH R. M., *J. Phys.: Condens. Matter*, **21** (2009) 395502.
- [19] SHELLEY M., *Theory and simulation of semiconducting nanowires for thermoelectric applications* Ph.D. thesis Imperial College London (2011).
- [20] MARZARI N. and VANDERBILT D., *Phys. Rev. B*, **56** (1997) 12847.
- [21] CAROLI C., COMBESCOT R., NOZIERES P. and SAINT-JAMES D., *J. Phys. C: Solid State Phys.*, **4** (1971) 916.
- [22] LEE D. H. and JOANNOPOULOS J. D., *Phys. Rev. B*, **23** (1981) 4988; **23** (1981) 4997

- [23] MEIR Y. and WINGREEN N. S., *Phys. Rev. Lett.*, **68** (1992) 2512.
- [24] NARDELLI M. B., FATTEBERT J. and BERNHOLC J., *Phys. Rev. B*, **64** (2001) 245423.
- [25] SIVAN U. and IMRY Y., *Phys. Rev. B*, **33** (1986) 551.
- [26] ESFARJANI K., ZEBARJADI M. and KAWAZOE Y., *Phys. Rev. B*, **73** (2006) 085406.
- [27] KIM R., DATTA S. and LUNDSTROM M. S., *J. Appl. Phys.*, **105** (2009) 034506.
- [28] WANG S. and MINGO N., *Phys. Rev. Lett.*, **79** (2009) 115316.
- [29] WANG J.-S., WANG J. and LU J. T., *Eur. Phys. J. B*, **62** (2008) 381.
- [30] YAMAMOTO T. and WATANABE K., *Phys. Rev. Lett.*, **96** (2006) 255503.
- [31] TERSOFF J., *Phys. Rev. B*, **37** (1988) 6991; **39** (1989) 5566
- [32] MARKUSSEN T., JAUHO A. and BRANDBYGE M., *Nano Lett.*, **8** (2008) 3771.
- [33] WEN C., REUTER M. C., BRULEY J., TERSOFF J., KODAMBAKA S., STACH E. A. and ROSS F. M., *Science*, **326** (2009) 1247.
- [34] MARKUSSEN T., RURALI R., JAUHO A.-P. and BRANDBYGE M., *Phys. Rev. Lett.*, **99** (2007) 076803.
- [35] MARKUSSEN T., JAUHO A. and BRANDBYGE M., *Phys. Rev. B*, **79** (2009) 035415.
- [36] LEVINE D. and STEINHARDT P. J., *Phys. Rev. Lett.*, **53** (1984) 2477.
- [37] POPE A. L. and TRITT T. M., *Thermal conductivity of quasicrystalline materials* in *Thermal Conductivity*, edited by TRITT T. M., (Springer) 2004 pp. 255–259.